

CHARACTERIZATION OF UNORDERED CARBON USING WARREN-BODENSTEIN'S EQUATION

*Hiroyuki Fujimoto and Minoru Shiraishi**

R & D Department, Osaka Gas Co., Ltd.

6-19-9, Torishima Konohana-ku Osaka 554-0051, Japan

**School of high-technology for human welfare, Tokai University*

317, Nishino, Numazu, Shizuoka 410-0395, Japan

Introduction

In 1950's, Diamond proposed an estimation method of carbon layer size distribution for carbonized coal by analyzing the x-ray scattering intensity[1-4]. In his method, the observed 11 band profile of carbon was fitted by the summation of weighted theoretical intensities in electron unit, I_{eu} of several model carbon layer planes with different sizes based on Debye's scattering equation.

$$I_{eu}(s) = \sum_i \sum_j f^2(s) \frac{\sin 2\pi s r_{ij}}{2\pi s r_{ij}} \quad (s = 2 \sin \theta / \lambda) \quad (1)$$

where 2θ , λ , f and r_{ij} are the diffraction angle, wave length of x-ray, atomic scattering factor and inter-atomic distance of two atoms, i and j . A lot of useful information has been obtained concerning the structures of coal and amorphous polymers composed of aromatic carbons by the method[1-7]. Strictly speaking, Diamond's theory is only applicable for a sample containing only single layers. However, Warren & Bodenstein pointed out that, for samples in which there are parallel layer groups containing several layers, there will also be (00 l) reflections, and additional modulations which affect the shape of the (hk) reflections and that, to have a rigorous representation of features such as peak breadths and peak displacements, it is desirable to extend Diamond's treatment to include the case of parallel layer groups containing several layers[8]. They considered the interaction between a layer and the p th nearest neighbor layer and, proposed a developed

equation concerning the coherent scattering intensity of parallel layer groups with the number of carbon layer plane stacked, M and carbon atoms in a plane, N by

$$I_{eu}(s) = M \sum_i \sum_j f^2(s) \frac{\sin 2\pi s r_{ij}}{2\pi s r_{ij}} + 2 \sum_p \sum_i \sum_j (M - p) f^2(s) \frac{\sin 2\pi s r_{ij}}{2\pi s r_{ij}} \quad (2)$$

If we apply Warren-Bodenstein's equation (WB's equation) instead of Debye's equation in Diamond's method, not only the 11 band fitting but also the whole powder pattern fitting will be possible. This technique suggests that the distribution of carbon layer stacking along c -axis as well as that of carbon layer plane size along a, b -axis are obtained at the same time. That is, the crystallite size distribution along a, b - and c -axes can be two-dimensionally analyzed. In the present study, the theoretical scattering intensities of several hundreds of carbon model crystallites were calculated using Warren-Bodenstein's equation and the observed x-ray diffraction pattern of mesocarbon microbeads (MCMBs) were refined by the least square method using the calculated intensities. Based on the result, the usefulness of two-dimensional analysis of carbon will be discussed.

Analysis procedure

In eq.(2), the first term denotes the coherent scattering by a carbon atom itself and by two atoms with an inter-atomic distance of r_{ij} in a carbon layer plane, and second one, the coherent scattering by the two

carbon atoms with an inter-atomic distance of r_{ij} in different layer planes. Now, we consider a crystallite model based on the benzene ($n=0$) and coronene ($n=1$) structures as shown in Fig.1[9,10]. Since there are $(2n+1)$ hexagons along a-axis, the crystallite sizes, La and Lc and the number of carbon atoms in a layer plane are expressed with the lattice constants and interlayer spacing, a_0 and $c_0=2d_{002}$ by

$$La = a_0(2n+1), \quad Lc = d_{002}(M-1), \quad N = 6(n+1)^2 \quad (5)$$

In the present study, the above hexagonal crystallite model was applied for calculating the theoretical intensities of carbons with different crystallite sizes in the range of $a_0 < La < 31a_0$, ($n = 0, 1, \dots, 15$) and $0 < Lc < 14d_{002}$, ($M = 1, 2, \dots, 15$), where a_0 and d_{002} were treated as variables in the range of 0.344-0.389nm and 0.2431-0.2461nm, respectively.

In Fig.1, let the origin be on the center of carbon layer plane, and the coordinates of all atoms in a carbon layer plane are written with arbitrary integers, m_1 and n_1 by

$$\begin{aligned} &((m_1 + 1/3)a_0, (n_1 + 2/3)a_0) \text{ and} \\ &((m_1 + 2/3)a_0, (n_1 + 1/3)a_0) \quad (6) \end{aligned}$$

$$\text{when } 0 \leq n_1 \leq n, \quad -n + n_1 \leq m_1 \leq n$$

$$\text{when } -n \leq n_1 < 0, \quad -n \leq m_1 \leq n + n_1$$

Hence, the first term in eq. (2) can be exactly calculated even with Pentium III processor level when La is smaller than ca.5 nm. However, the calculation of the second term requires enormous time in case of a large crystallite size. Warren & Bodenstein proposed a disk shape crystallite and derived a Fourier transform geometrically from the second term and finally obtained a following equation as the coherent scattering per atom, I_{coh} .

$$\begin{aligned} I_{coh}(s) = \frac{I_{eu}(s)}{MN} = \frac{1}{N} \sum_i \sum_j f^2(s) \frac{\sin 2\pi s r_{ij}}{2\pi s r_{ij}} \\ + 2 \sum_p f^2(s) \left(1 - \frac{p}{M}\right) \cdot i(p) \quad (7) \end{aligned}$$

$$i(p) = \frac{0.2427}{s} \int_{pd_{002}}^{r_m} \left\{ \arccos u - u(1-u^2)^{1/2} \right\} \sin 2\pi s r dr \quad (8)$$

$$r_m = \left\{ La^2 + (pd_{002})^2 \right\}^{1/2} \quad (9)$$

$$u = \sqrt{r^2 - (pd_{002})^2} / La \quad (10)$$

On the other hand, the incoherent scattering per atom, I_{inc} is approximated by Hajdu's equation[11] multiplied by Ruland's attenuation function, $Q(s/2)$ [12].

$$\begin{aligned} I_{inc}(s/2) = \left(A - \frac{f^2(s/2)}{A} \right) \\ \times [1 - B\{\exp(-Cs/2) - \exp(-Ds/2)\}] \times Q(s/2) \quad (11) \end{aligned}$$

$$A=6, B=0.4972, C=1.8438, D=7.8917$$

If the background scattering is neglected, the total scattering intensity, $B(s)$ of a carbon crystallite with known crystallite size is written by

$$B(s) = K \{ I_{coh}(s) + I_{inc}(s) \} A(s) P(s) \quad (12)$$

where K , $A(s)$, $P(s)$ are the scale factor, absorption factor, polarization factor, respectively. Hence, if the crystallite sizes, La and Lc are given in advance, the theoretical intensity can be computed by the combination of eqs.(7), (11) and (12). Now, we postulate the real carbon is composed of q crystallites with different La and Lc , the observed scattering intensity, $I(s)$ is expressed with the error function, $v(s)$ by

$$I(s) = \sum_{i=1}^q w_i B_i(s) + v(s) \quad (13)$$

where w_i is the scale factor of intensity for the i th crystallite. The least square refinement to minimize the summation of squared errors,

$$\varepsilon^2 = \sum_s v^2(s) = \sum_s \left(I(s) - \sum_i w_i B_i(s) \right)^2 \quad (14)$$

gives the optimized parameters, w_i . Therefore, the average crystallite size $\langle La \rangle$, $\langle Lc \rangle$ and the fraction of each component crystallite, c_i are calculated as follows.

$$\langle La \rangle = \frac{\sum_i w_i La_i}{\sum_i w_i}, \quad \langle Lc \rangle = \frac{\sum_i w_i Lc_i}{\sum_i w_i},$$

$$c_i = \frac{w_i}{\sum_i w_i} \times 100 \quad (15)$$

In order to determine w_i under the condition that each w_i is non-negative, the steepest descent method, one of the conventional least square method was applied[14].

Firstly, we assume the q -dimensional space for $\mathcal{E}^2(w_1, w_2, \dots, w_q)$ which is a function of parameters w_1, w_2, \dots, w_q and let \mathbf{X} and \mathbf{x}_1 the point with minimum value of \mathcal{E}^2 and an arbitrary start point, respectively, where all the parameters are non-negative, respectively. Secondary, we determined the point \mathbf{x}_2 which is the nearest point to \mathbf{x}_1 along the steepest descent direction at \mathbf{x}_1 , $-\nabla \mathcal{E}^2(\mathbf{x}_1)$ and is related to \mathbf{x}_1 by

$$\mathbf{x}_2(t) = \mathbf{x}_1 - t \nabla \mathcal{E}^2(\mathbf{x}_1) \quad (16)$$

where t is a coefficient in the range of $0 < t < 1$. The value of t and the point of $\mathbf{x}_2(t)$ can be determined under the condition of

$$\partial \mathcal{E}^2(\mathbf{x}_2(t)) / \partial t = 0 \quad (17)$$

After the determination of t and \mathbf{x}_2 , the point \mathbf{x}_1 was displaced by the point \mathbf{x}_2 . Then, the above mentioned procedure was repeated by 2000 times to determine the point \mathbf{X} . If the calculation result by 2000 times repeats contained any negative parameters, all the parameters were recalculated after excluding the negative ones, because it was considered that the crystallite models corresponding such parameters were not contained in the samples. The fitting accuracy was estimated by R-factor.

$$R = \sum_s \left| I(s) - \sum_i w_i B_i(s) \right| / \sum_s I(s) \times 100 \quad (18)$$

The above mentioned calculation was carried out on Windows 98 with a CPU of Intel Pentium III processor

(550MHz) using Visual Basic 6.0 as a programming language. The program is named "Carbon Analyzer 98" and its outline for the numerical treatment is visually shown on the Web site (<http://www.asahi-net.or.jp/~qn6h-fjmt/index.htm>)

Experimental

MCMBs heat-treated were used for the present analysis, which were carbonized at the temperature range of 700 - 1400°C under Ar atmosphere in a muffle furnace heated up to each temperature at 2.5 °C/min with soak time of 1 hr at the temperature. Hereafter, the MCMBs heat-treated is abbreviated to "MC" and followed by its heat treatment temperature, for instance, "MC900" for the specimen heat-treated at 900°C. The x-ray diffraction profiles of MCMBs heat-treated were measured with $\text{CuK}\alpha$ using RINT2500 diffractometer (Rigaku Denki Co., Ltd.). The measurement was carried out by a step-scanning technique with an interval of 0.1°. The integral width of energy pass-band function was approximated to be 0.05. The accumulation time was adjusted so that the maximum intensity obtained was several thousands counts. The tube-voltage and current were 40 kV and 200 mA, respectively. The diffraction profiles obtained were fitted by the steepest descent method.

Results and discussion

Figures 2 and 3 show the calculated intensities in the case of fixed La and varied Lc , and varied La and fixed Lc . Figure 4 shows those in cases of fixed La and Lc and varied d_{002} . One can see that the intensities of (00 l) and (hk) reflections increased with increasing the Lc and La sizes, respectively and that the 002 peak become intense and shift to lower side of diffraction angle with increasing the value of d_{002} . This is due to the increase of integration range in eq.(8). In

the range of $2\theta < 20^\circ$, remarkable oscillations which were part of the interference function for thin crystallites. Such oscillations will be averaged out by a small range of L_c values. For the observed intensities, there will also be an appreciable contribution of small angle scattering in lower angle than the vicinity of 002 line. Hence, the least square refinement was carried out in the range of $20^\circ < 2\theta < 100^\circ$ in order to avoid these effects.

Figure 5 shows the fitting results of profiles of MCMBs heat-treated with different temperatures. The bold and thin lines denote the observed and fitted profile, respectively. The residual curve is also shown in the upper part of the profile. In all the profiles, the fitting accuracy of 004 and 110 peaks was lower than that of 002 and 100. It would be due to the lowering of observed intensity by the thermal vibration effect which was not considered in eq.(7). Secondary, since the least square fitting was carried out with no consideration of small angle scattering which exists in the range of $0^\circ < 2\theta < 25^\circ$, the 002 profile of the fitting curve was overestimated. Hence, the (004) reflection would also be overestimated correspondingly.

R-factor of MCMBs becomes minimum at the heat treatment temperature of 1000°C in the range of $700\text{-}1400^\circ\text{C}$. In the earlier stage of heat-treatment, MCMBs contains pyrene-based skeleton structures, hetero atoms and cross-linking bonds which are not considered in the benzene- and coronene-based skeleton structure used in the present study. Therefore, the R-factor of MC700 is larger than that of MC1000. On the other hand, above 1200°C , the graphitizability (degree of misorientation) will be gradually enhanced by the acceleration of crystallite growth. Since WB's equation is derived with no consideration of ABAB stacking of carbon layer planes, the x-ray profile calculated from WB's equation is close to that of turbostratic carbon. This will be the reason that makes the R-factor lower.

Figures 6 and 7 shows the crystallite size

distribution histograms of MCMBs heat-treated at $700\text{-}900^\circ\text{C}$ and $1000\text{-}1400^\circ\text{C}$ obtained from the least square fitting. The accumulation histograms projected onto the L_a - and L_c -axes are also shown on the wall of three-dimensional graphs. They must be theoretically the same as those obtained by Diamond's method and Hirsch's method which describe the carbon layer plane distribution and layer stacking distribution, respectively[1-7,13].

(i) Temperature range of $700\text{-}900^\circ\text{C}$

For MC700, along a-axis, carbon layer planes in crystallite units composed of 2-4 layers distribute in the range of $0.5\text{-}2.7\text{nm}$. Along c-axis, the number of carbon layer stacking distributes in the range of $0\text{ nm} < L_c < 4.2\text{ nm}$ (1 – 15 sheets of carbon layer plane), while the samples of MC800 and MC900 exhibits two peaks, a main peak by 2-4 layers units and a shoulder peak by 6-8 layers units and the units composed of more than 10 layers hardly exist. In this temperature range, the carbon layer stacking distribution is once disturbed by the diffusion of decomposition gas accompanied by the polymerization or condensation to form a lot of 2-4 layers units, and then, such units will coalesce each other to form 5-8 layers units.

Above 800°C , the carbon layer plane continues to gradually develop. As a result, the van der Waals force also increases and the single layers gradually disappear. The noticeable point is that the amount of 5-layers unit is smaller than those of 6 or 7 layers units. It indicates that the 2-4 layers units meet each other and coalesce to grow 6-8 layers unit. Then, 2-4 layers and 6-8 layers units might coalesce to grow 10 layers unit. If such a coalescence mechanism continue to occur even at higher temperatures, the possible main stacking number may be a magic number such as 2, 3, 7, 10, 13, 17, ...

(ii) Temperature range of $1000\text{-}1400^\circ\text{C}$

Above 1000°C , the continuative growth of carbon layer plane accompanying the increase of van

ver Waals force between the layers results in the increase of the stacking number. Hence, the 2 layers unit finally disappears and the coalescence of the units is accelerated. In this temperature range, two peaks by the 2-4 layers units and 6-8 layers units are also observed in the carbon layer stacking distribution.

Figure 8 shows the average crystallite size estimated from eq.(14). The L_a size increases monotonously, while the L_c size once decreases slightly at 800-900°C and increases again. The tendency is the same as that previously estimated from the half width of the 002 and 110 peak using Si as an internal standard[10].

As mentioned above, the accumulation histograms projected onto L_a - and L_c - axes in Figs.6 and 7 must be equivalent to the histograms obtained from the theories of Diamond and Hirsch, respectively.

The projected histogram onto L_a -axis for MC800 was compared with the carbon layer size distribution given by Diamond's method in Fig.9. Both distributions are quite different. In the latter method, only 11 band with the weakest intensity in the profile was fitted with no consideration of the incoherent scattering and coherent scattering by the parallel layer groups, while in the former, whole powder pattern was fitted considering not only 110 band but also 002, 004, 100. And also, as mentioned in Section 4.2, the effect of thermal vibration become remarkable in the 11 band resulting the lowering of the observed intensity. Hence, the two-dimensional analysis gives a higher accuracy than Diamond's method.

Figure 10 shows the projected histogram onto L_c -axis for MC800 compared with the carbon layer stacking distribution estimated by Hirsch's method[14]. In the former method, the distribution shape largely depends on the fitting accuracy of profile. In Hirsch's treatment, the 002 profile is Fourier-transformed based on the theory of Patterson function. Hence, the amount of single layer can not be estimated. The result of

Fourier transform is remarkably affected by how to extrapolate the scattering intensity to zero angle and by how to subtract the background. The difference of the distribution shape between the both methods might come from such delicate numerical treatments.

Conclusion

The x-ray diffraction profile of carbon could be refined by the steepest descent method, one of the conventional least square refinement using several hundreds of theoretical scattering intensities of crystallites calculated from WB's equation and it made possible to estimate the crystallite size distribution two-dimensionally along L_a - and L_c -axes. As a result, for the MCMBs heat-treated at 700-1400°C, it was clarified that carbon layer planes grow gradually and were stacked by the van der Waals force to form the 2-4 layers units in the earlier stage of the heat treatment. Then, they coalesce each other along c -axis to form 6-8 layers units.

References

1. Diamond R. X-ray studies of some carbonized coals. England, Univ. of Cambridge, PhD Dissertation, 1956.
2. Diamond R. X-ray diffraction data for large aromatic molecules. Acta Cryst. 1957; 10: 359-364.
3. Diamond R. A least-squares analysis of the diffuse x-ray scattering from carbons. Acta Cryst. 1958; 11: 129-138.
4. Diamond R. X-ray studies of some carbonized coals. Phil. Trans. Roy. Soc. London 1960; A252: 193-223.
5. Brooks JD, Stephens JF. A test of Diamond's method for estimating size distribution of aromatic ring systems. Carbon 1965; 2: 379-384.
6. Shiraishi M, Kobayashi K. An x-ray study of coal

tar pitch. Bull. Chem. Soc. Japan 1973; 46: 2575-2578.

7. Fujimoto H, Shiraishi M. Analysis of carbon layer size distribution of MCMB by the method proposed by Diamond. Tanso 1999; 187: 83-87.
8. Warren BE, Bodenstern P. The diffraction pattern of fine particle carbon blacks. Acta Cryst. 1965;18: 282-286.
9. Fujimoto H, Mabuchi A, Tokumitsu K, Kasuh T, Akuzawa N. Effect of crystallite size on the chemical composition of the stage 1 alkali metal-graphite intercalation compounds. Carbon 1994;32(2): 193-198.
10. Fujimoto H, Mabuchi A, Tokumitsu K, Kasuh T, Shiraishi M. New structural parameters for carbon:

comprehensive crystallization index and cavity index. Carbon 1994;32(7): 1249-1252 .

11. Hajdu F. Revised parameters of the analytic fits for coherent and incoherent scattered x-ray intensities of the first 36 atoms. Acta Cryst. 1972;A28: 250-252.
12. Ruland W. The separation of coherent and incoherent Compton x-ray scattering. Brit. J. Appl. Phys. 1964; 15:1301-1307.
13. Hirsch PB. X-ray scattering from coals. Proc. Roy. Soc. 1954;A226: 143-169.
14. Fujimoto H, Shiraishi M. Analysis of stacking structure of mesocarbon microbeads: Patterson function method and its reliability. Tanso 1995; 167: 101-107.

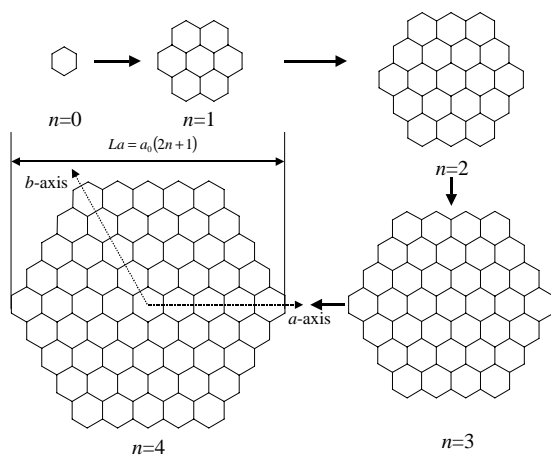


Fig.1 Crystallite model based on benzene and coronene structure used in the present study

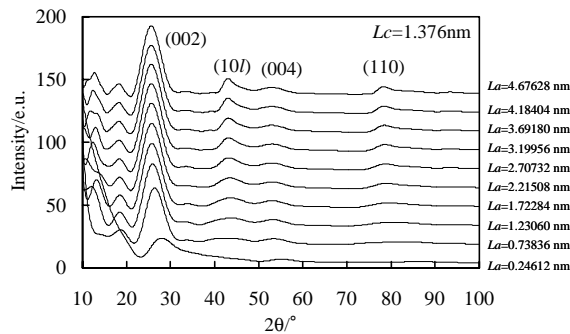


Fig.3 The dependence of scattering intensity on the crystallite size on L_a for fixed L_c

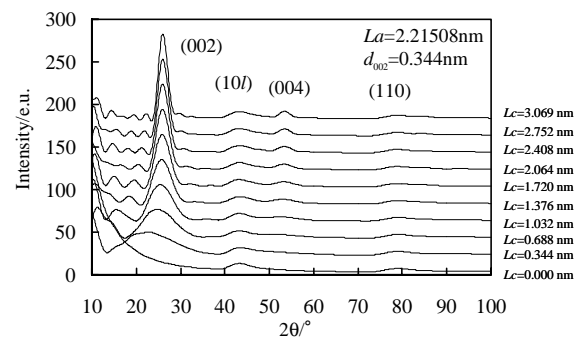


Fig.2 The dependence of scattering intensity on the crystallite size on L_c for fixed L_a

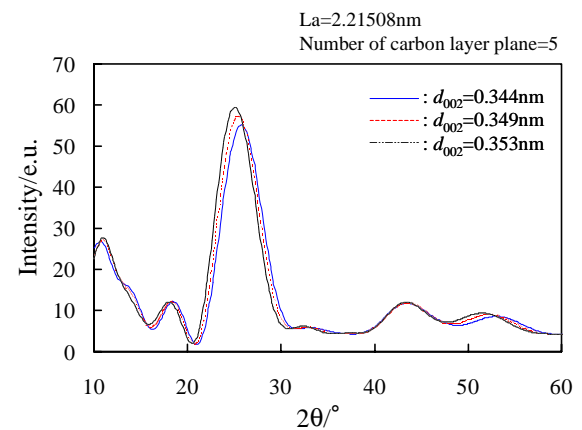


Fig.4 The dependence of scattering intensity on the interlayer spacing for fixed L_c and L_a

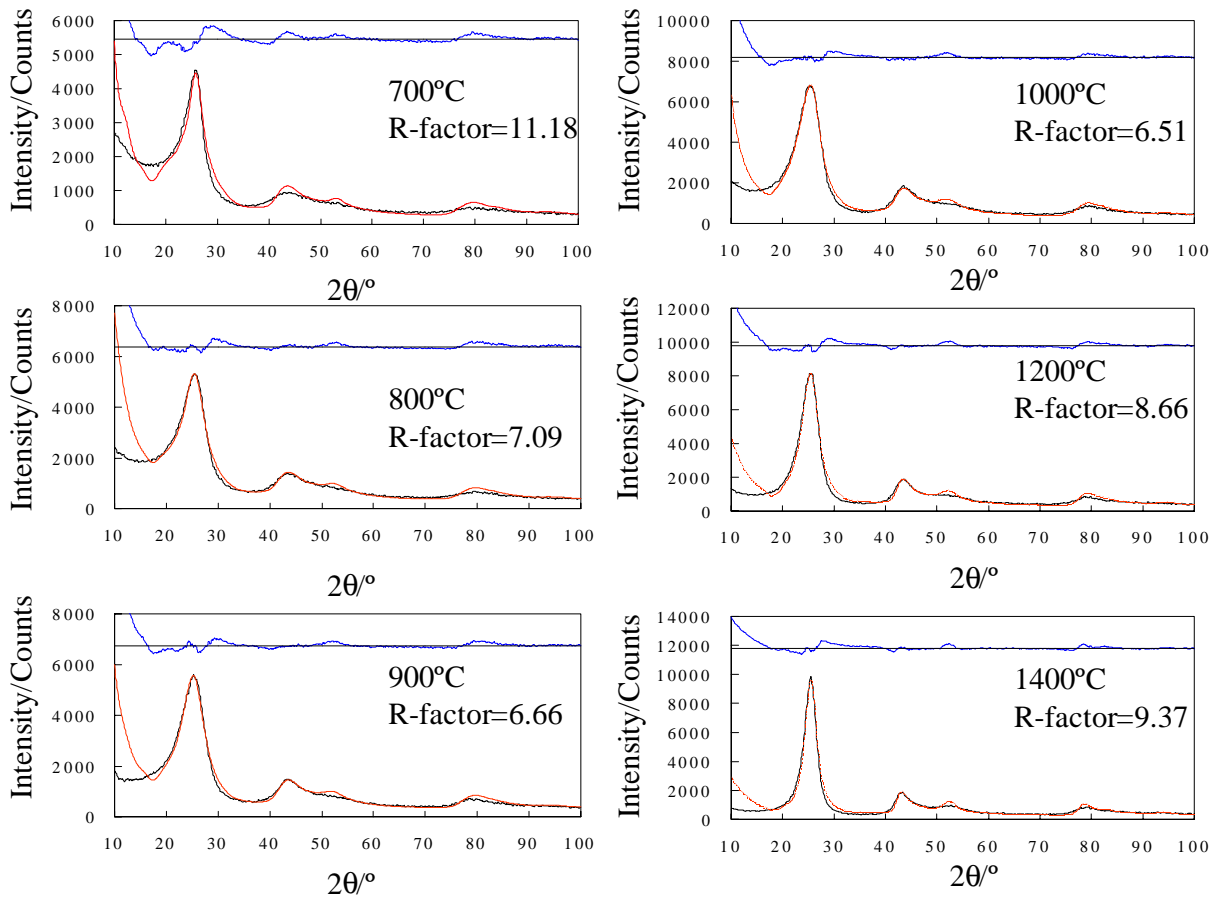


Fig.5 The results of the least square refinement of x-ray diffraction profiles of MCMBs heat-treated at several temperatures

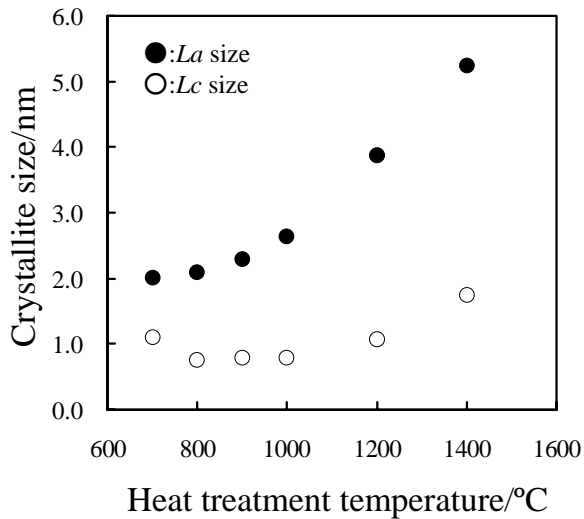


Fig.8 Average crystallite size at different heat treatment temperatures

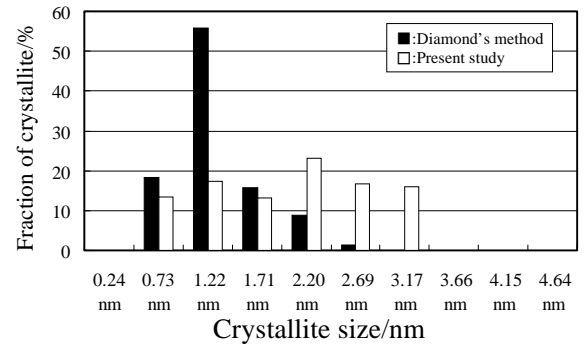


Fig.9 The distribution of carbon layer plane size estimated from the present study and from Diamond's method for the sample of MCMB heat-treated at 800°C

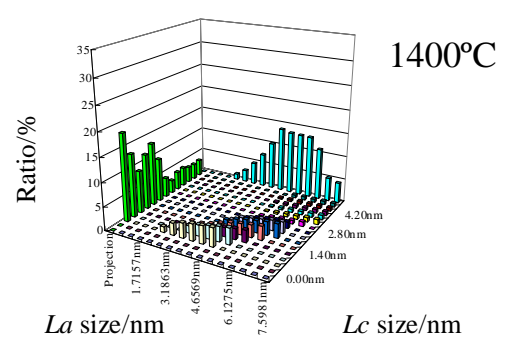
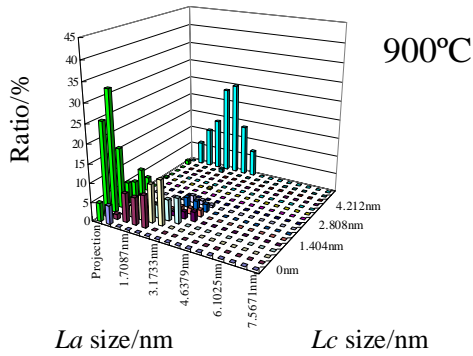
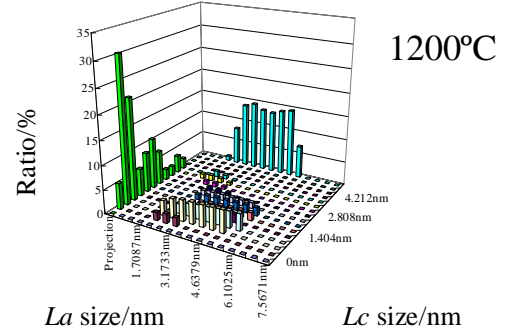
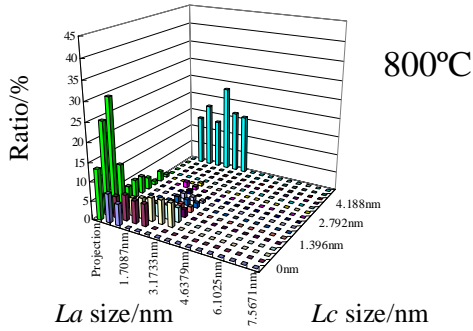
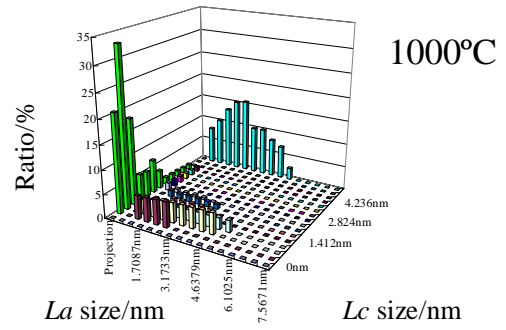
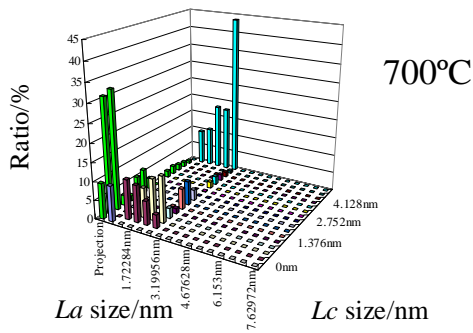


Fig.6 Two-dimensional crystallite size distribution of MCMBs heat-treated at several temperatures

Fig.7 Two-dimensional crystallite size distribution of MCMBs heat-treated at several temperatures

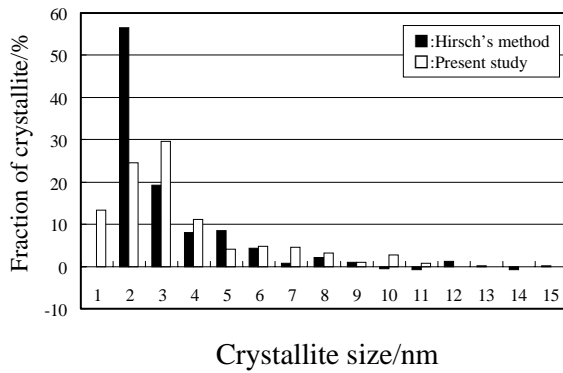


Fig.10 The distribution of carbon layer stacking number estimated from the present study and from Hirsch's method for the sample of MCMB heat-treated at 800°C